ELSEVIER

Surface Science 304 (1994) 267–280

surface science

Coverage-dependent adsorption sites for K/Cu(001) and Cs/Cu(001) determined by surface X-ray diffraction

H.L. Meyerheim [a,*], J. Wever [a], V. Jahns [a], W. Moritz [a], P.J. Eng [b], I.K. Robinson [b]

[a] *Institut für Kristallographie und Mineralogie der Universität München, Theresienstrasse 41, 80333 München, Germany*
[b] *Department of Physics, University of Illinois, Urbana, IL 61801, USA*

(Received 26 August 1993; accepted for publication 16 November 1993)

Abstract

Surface X-ray diffraction has been used to analyze in situ the room-temperature adsorption behaviour and the structure of K and Cs on Cu(001) at submonolayer coverages. Adsorption of K takes place in fourfold hollow sites up to coverages of about 0.25 monolayers (ML), where 1 ML corresponds to 1.53×10^{15} atoms/cm^2. At higher coverages the formation of a quasi-hexagonal incommensurate adlayer is observed. In contrast, for Cs adsorption we observe from the very beginning the formation of the quasi-hexagonal structure up to the completion of the adlayer at about 0.30 ML. For K adsorption in the hollow sites we determine an adsorption height, $d_\perp = 2.25(15)$ Å, corresponding to an effective K radius of $r_{\text{eff}} = 1.6(1)$ Å close to the ionic radius of 1.33 Å. We do not observe a change in the effective radius as a function of coverage. For the quasi-hexagonal Cs structure we find an (average) adsorption height $d_\perp = 2.94$ Å corresponding to an effective radius of $r_{\text{eff}} = 2.18$ and 1.93 Å, for the limiting cases of hollow- and bridge-site adsorption, respectively. The analysis of the superlattice reflections corresponding to the quasi-hexagonal incommensurate structures indicated that the K adlayer is strongly modulated. The first Fourier component of the substrate-induced modulation was determined to $u_{01} = 1.29(3)$ Å. In contrast, for Cs/Cu(001) static modulation is much less important ($u_{01} \leq 0.2$ Å). Variation of the Cs adlayer density by changing the substrate temperature allows continuous expansion and contraction of the adsorbate unit cell. No commensurate–incommensurate transition has been observed.

1. Introduction

There is a long-standing debate about the bonding character of alkali atoms adsorbed on metal surfaces. The traditional view is that an alkali atom adsorbed at low coverages transfers its valence electron at least partially to the metal to become ionic. At higher coverages depolarization of the dipoles leads to the formation of an alkali overlayer that is covalently bonded to the substrate atoms. This model was inferred by Langmuir and Kingdon in 1923 [1]. One prominent feature of alkali adsorption related to this "charge transfer" and "charge back-donation" model is the decrease in the workfunction, which passes a minimum at about 0.20 monolayers (ML, 1 ML = 1.53×10^{15} atoms/cm^2), which subsequently increases to saturation corresponding to the workfunction of the alkali metal.

* Corresponding author.

SSDI 0039-6028(93)E0955-T

On the other hand, both theoretical [2] and experimental [3] investigations support a picture of covalent bonding at all coverages. This is in contrast to recent calculations by Scheffler et al. [4] and by Pacchioni et al. [5] which, although entirely different in their theoretical approach, consistently attribute only a small covalent bonding character at low coverages. However, it should be noted that the distinction between ionic and covalent bonds might be semantic in nature, especially if there is a large overlap of the charge distributions of adsorbate and substrate.

Besides theoretical calculations and experiments concerned with the electronic structure, analyses of the geometric structure are helpful in order to obtain a complete picture of the alkali adsorption. However, precise structural data are rare. Low-energy electron diffraction (LEED) studies have been confined to investigations of ordered superstructures [6–16] thus providing only information about the high alkali coverage regime. This shortcoming might be removed by the development of the diffuse LEED (DLEED) technique [17], although this is still at an early stage. Another complication may arise from the contamination rate of the surface which is increased by the electron beam as well as by electron-stimulated desorption.

X-ray scattering data on surfaces can be interpreted in terms of the kinematical diffraction theory [18,19] and can be applied to the determination of the registry of the adlayer relative to the surface even in cases where no ordered superlattice structure has been formed.

Table 1
Structural determinations for alkali metal adsorption on unreconstructed metallic surfaces

System	Coverage (ML)	Site	Method	r_{eff}	r_{ion}	$r_{met.}$	Reference
Cs/Ag(111)	0.15	–	SEXAFS	1.76(3)	1.67	2.68	[21]
Cs/Rh(100) c(4 × 2)	0.25	Hollow	LEED	2.10(6)	1.67	2.68	[6]
Cs/Ru(0001) p(2 × 2)	0.25	Top	LEED	1.90(8)	1.67	2.68	[7]
Cs/Cu(111) p(2 × 2)	0.25	Top	LEED	1.73(5)	1.67	2.68	[8]
Cs/Cu(001) c(2 × 10)	0.30	Hollow and Asymmetrical	X-ray	2.18(13) [a] 1.93(14) [b]	1.67	2.68	Present work
Cs/Ag(111)	0.30	–	SEXAFS	2.06(3)	1.67	2.68	[21]
Cs/Ru(0001)($\sqrt{3} \times \sqrt{3}$)	0.33	Hcp hollow	LEED	2.17(2)	1.67	2.68	[7]
Cs/Rh(100)($\sqrt{5} \times \sqrt{5}$)	0.40	Hollow and top	LEED	2.12	1.67	2.68	[11]
Cs/Rh(100) c($2\sqrt{2} \times 2\sqrt{(2/3)}$)R45°	0.43	Incommensurate	LEED	2.20	1.67	2.68	[11]
K/Cu(001)	0.14	Hollow	X-ray	1.5(3)	1.33	2.38	[20]
K/Cu(001)	0.25	Hollow	X-ray	1.6(1)	1.33	2.38	Present work
K/Cu(001) (C1-C2)	0.30–0.33	Incommensurate	X-ray	1.6(1)	1.33	2.38	Present work
K/Cu(111)p(2 × 2)	0.33	Top	SEXAFS	1.79(3)	1.33	2.38	[14]
K/Ni(100)	< 0.25	Hollow	DLEED [c]	2.02–1.97	1.33	2.38	[17]
K/Ni(100)c(4 × 2)	0.25	Hollow	LEED	1.96(5)	1.33	2.38	[13]
K/Ni(111)	0.13–0.28	Incommensurate	CMTA [d]	1.46(10)	1.33	2.38	[35]
K/Ni(111)p(2 × 2)	0.25	Top	LEED	1.57(3)	1.33	2.38	[12]
K/Ni(111)p(2 × 2)	0.25	Top	SEXAFS	1.67(2)	1.33	2.35	[14]
K/Co(10$\bar{1}$0)c(2 × 2)	0.50	Hollow	LEED	1.87(5)	1.33	2.38	[10]
K/Ru(001)$\sqrt{3} \times \sqrt{3}$	0.33	Hcp hollow	LEED	1.98(5)	1.33	2.38	[15]
K/Ru(001)p(2 × 2)	0.25	Fcc hollow	LEED	1.94(5)	1.33	2.38	[15]
K/Al(111)$\sqrt{3} \times \sqrt{3}$	0.33	Top	LEED	1.80(5)	1.33	2.38	[16]
K/Al(111)$\sqrt{3} \times \sqrt{3}$	0.33	Substitutional	LEED	2.10(3)	1.33	2.38	[16]

[a] Radius derived for hollow site.
[b] Radius derived for bridge site.
[c] Diffuse LEED.
[d] CMTA (constant momentum transfer averaging) of LEED intensities.

In a previous paper [20] we discussed in detail the structure of K layers adsorbed on Cu(001) at about 0.14 ML coverage where no ordered superstructure has been formed. A fourfold hollow-site adsorption at an adsorption height $d_\perp = 2.1(4)$ Å was found. This corresponds to an effective K radius of 1.5(3) Å, which is considerably lower than $r_{\text{eff}} = 1.96(5)$ Å derived by LEED for K adsorbed on Ni(001) forming an ordered c(4 × 2) superstructure at 0.25 ML [13].

On the basis of these results, one matter of concern was to answer the question of whether there is a coverage-dependent adsorption height that could be correlated with the charge back-donation mechanism. In a surface-extended X-ray absorption fine structure (SEXAFS) study on Cs/Ag(111) Lamble et al. [21] found an increase in the Cs–Ag bond from 3.20(3) Å at 0.15 ML to 3.50(3) Å at 0.30 ML. An overview of the results of structure determinations for K and Cs adsorbate systems on unreconstructed metal surfaces is given in Table 1.

The results of the present investigation show that for K/Cu(001) there is no coverage dependence of the effective radius within the error bars of about 0.15 Å. In addition, we show that the adsorption behavior of K and Cs is completely different, although the ordered superstructure formed at about 0.30 ML is reported to be basically the same.

In Fig. 1 we summarize the different structures as determined for K on Cu(001) by Aruga et al. [22] on the basis of their LEED study. At a coverage above 0.18 ML short-range order is observed, which is indicated by a diffuse ring of intensity. The formation of long-range order is reported to take place at $\theta = 0.28$ ML where a commensurate quasi-hexagonal superstructure is observed, labeled C1. It can be described as a c(2 × 10) superlattice as shown in Fig. 2. The alkali atoms within the unit cell are represented by hatched circles. This superstructure corresponds to a theoretical coverage of 0.30 ML. When the coverage exceeds ~0.30 ML the superstructure is compressed and another commensurate quasi-hexagonal structure is reported to form, labeled C2 by Aruga et al. [22]. It is equivalent to a (2 × 3) superstructure. At coverages above 0.33 ML the K monolayer undergoes a commensurate–incommensurate transition forming an unregistered hexagonal lattice (Fig. 1).

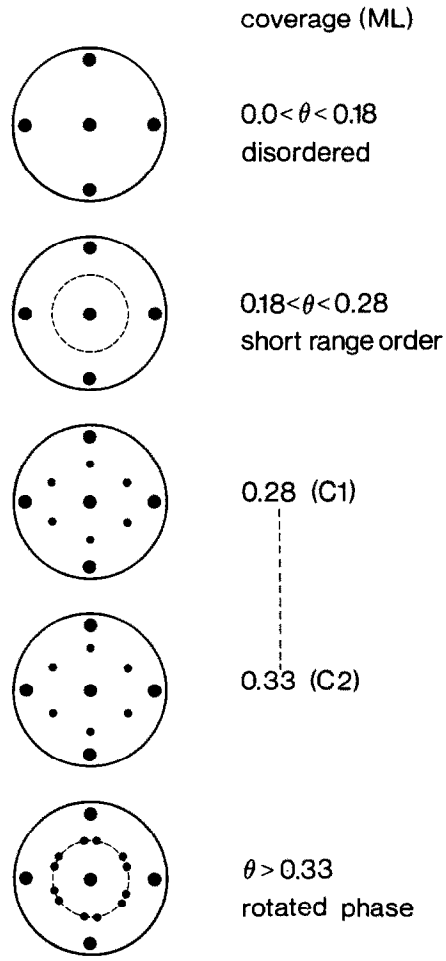

Fig. 1. Schematic representation of the LEED patterns for adsorption of K on Cu(001) as reported in Ref. [22]. Only one of two domains is shown.

The "phase diagram" for Cs/Cu(001) is very similar to those determined by Papageorgopolous et al. [23] and by Cousty et al. [24]. It is important to note that different substrate temperatures have been used in these investigations: 330 K for K/Cu(001) and 303 K for Cs/Cu(001). In our experiments we used the same temperatures as reported in the literature.

This paper is organized as follows. After a short discussion of the basic theory needed for

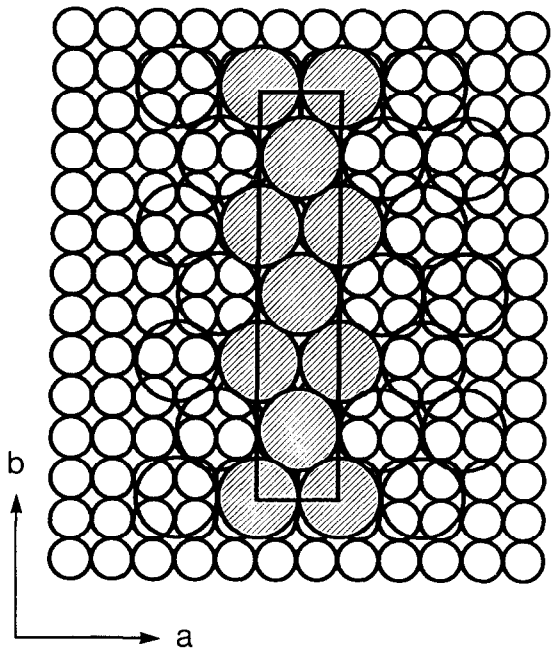

Fig. 2. Schematic representation of the commensurate quasi-hexagonal superstructure labeled C1 by Aruga et al. [22]. Using a rectangular setting of the unit cell this corresponds to a c(2×10) superstructure as indicated by the solid line. The alkali atoms within the unit cell are shown hatched.

the analysis of the truncation rod data in Section 2, we discuss in Sections 3 and 4 the adsorption behavior and the structure of K and Cs on Cu(001) as derived from the truncation rods. The analysis of the fractional-order superlattice reflections is presented in Section 5, and a short summary of the results is given in Section 6.

2. Theory

The analysis of the adlayer registry relative to the substrate is based on the interference of the scattering amplitudes from the substrate (F_{CTR}) and adsorbate (F_{Ad}): $F_{tot} = F_{CTR} + F_{Ad}$, where F_{CTR} is the structure factor of the diffuse intensity between the bulk Bragg points. It arises from the truncation of the (semi-infinite) crystal. Therefore, the rod of diffuse intensity is called the crystal truncation rod (CTR). For a more complete discussion, see e.g. Refs. [25–27].

In the present case we discuss the truncation rod of the Cu(001) surface. For convenience we use the primitive setting of the (001) surface unit cell corresponding to the tetragonal setting of the bulk unit cell [28].

The Cu(001) crystal is described as a semi-infinite stack of layers n from $n = -\infty$ to $n = 0$, the latter corresponding to the surface layer. The phase difference Ψ between the individual layers is given by $\Psi = \boldsymbol{q}\boldsymbol{r} = \pi(h + k + l)$, since the vector $\boldsymbol{r}$ between two consecutive layers is (1/2, 1/2, 1/2). Neglecting absorption, the total diffracted intensity can be expressed as:

$$I_{tot} = \left| f_{Cu} \sum_{n=-\infty}^{n=0} e^{in\Psi} + \theta f_{Ad}\, e^{i2\pi(hx+ky+lz)} \right|^2 . \quad (1)$$

The semi-infinite series can be evaluated leading to:

$$I_{tot} = \left| \frac{f_{Cu}}{1 - e^{-i\pi(h+k+l)}} + \theta f_{Ad}\, e^{i2\pi(hx+ky+lz)} \right|^2 , \quad (2)$$

where f_{Cu} and f_{Ad} represent the atomic form factors of the Cu substrate and the adlayer, respectively. The relative coverage of the adsorbate is described by θ. The position of the adatoms within the surface unit cell is given by the coordinates (xyz).

As the penetration of the X-rays is in the order of 1 μm, it is reasonable to extend the series to infinity since the error due to the finite penetration of the X-rays is negligible for $\boldsymbol{q}$ vectors far away from bulk reciprocal lattice vectors given by the condition $h + k + l = 2m$ (m integer).

It is important to note that surface sensitivity is only achieved far from the bulk Bragg points where the substrate lattice planes do not scatter in phase. For example, at the "anti-Bragg" condition, $h + k + l = 2m + 1$, the total scattering amplitude of the Cu substrate is given by $F_{CTR} = f_{Cu}/2$, which corresponds to half an atomic layer.

3. Adsorption of K and Cs on Cu(001)

The experiments were performed at the beamline X16A of the National Synchrotron Light

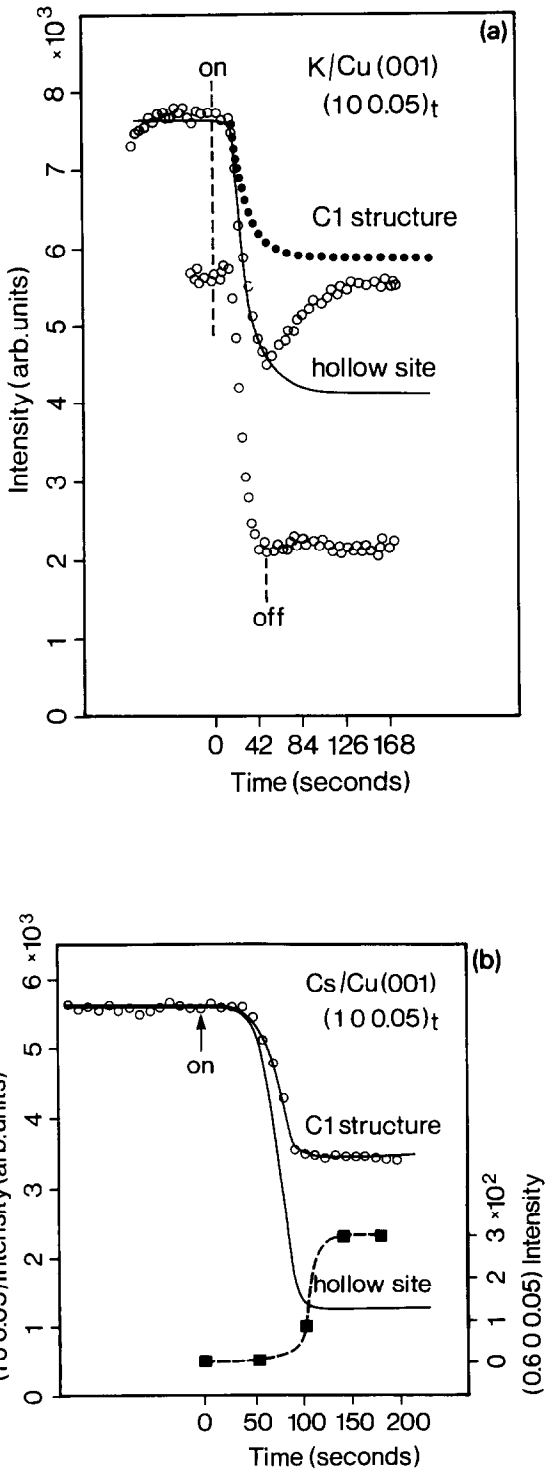

Source storage ring using the UHV diffractometer described in detail by Fuoss et al. [29] and Vlieg et al. [30]. The Cu(001) surface was prepared by repeated cycles of Ar^+ sputtering (500 eV) at a sample temperature of about 800 K, followed by several minutes of annealing at about 700 K. Adsorption of K and Cs was performed in situ using SAES dispensers mounted in front of the sample. The substrate temperature was about 303 K for Cs adsorption and 330 K for K adsorption. During the experimental runs the alkali sources were kept at a constant current of about 4 A below the emission temperature. Evaporation was started by increasing the current to 6 A. The constancy of the alkali emission rate was monitored by Auger electron spectroscopy.

Slits of 2×10 mm were mounted 500 mm behind the sample, providing a longitudinal resolution of 2.6×10^{-3} Å^{-1}. The resolution parallel to the truncation rods was $\Delta q_{\perp} = 1.3 \times 10^{-2}$ Å^{-1}, corresponding to about 0.05 reciprocal lattice units ($\lambda = 1.56$ Å).

Fig. 3(a) shows for adsorption of K on Cu(001) the measured intensity monitored in situ at $(10\,0.05)_t$, close to the antiphase condition $(100)_t$ along the $(10l)_t$ truncation rod. The left line indicates the moment at which the current of the SAES dispenser was increased to 6 A. For the lower curve (shifted down for clarity) the right line indicates the moment where the evaporation source was switched off.

Fig. 3. (a) $(10\,0.05)_t$ truncation rod intensity versus time for adsorption of K on Cu(001). The dashed lines indicate the moments where the evaporation sources have been switched on and off, respectively. The decrease and subsequent increase in the intensity can be explained by adsorption in hollow sites followed by formation of a quasi-hexagonal incommensurate overlayer. The dotted line shows the calculated intensity for the commensurate superstructure shown in Fig. 2. The lower curve is shifted down for clarity. (b) $(100.05)_t$ truncation rod intensity versus time for adsorption of Cs on Cu(001). The reduction to about 60% of the initial intensity is correlated with the formation of the quasi-hexagonal superstructure shown in Fig. 2. Assuming unique hollow-site adsorption, this is calculated to lead to a reduction to about 20% of the initial intensity. The filled squares represent the intensity of the first-order superlattice reflections $(0\,0.607\,0.05)_t$

We observe a rapid decrease in the diffracted intensity after about 20 s. The intensity decreases to about 52% of its original value after about 40 s. Stopping the evaporation leads to no further changes (lower curve), whereas continued evaporation results in a subsequent increase in the intensity, which asymptotically reaches about 75% of the original intensity (upper curve). The decrease and the subsequent increase in the intensity can be related to the occupation of fourfold hollow sites and to the formation of the incommensurate quasi-hexagonal K overlayer reported by Aruga et al. [22]. The corresponding superlattice reflections were observed after saturation of the $(10\,0.05)_t$ intensity. The decrease in the $(100)_t$ total intensity by occupation of hollow sites is easily explained by Eq. (2) (we neglect the small deviation of our data from the antiphase condition $(100)_t$). For K adsorbed in hollow sites $(1/2, 1/2, z)$ of the surface unit cell we obtain:

$$I_{\mathrm{tot}}(100) = \left|\tfrac{1}{2}f_{\mathrm{Cu}} + f_{\mathrm{K}}\theta\ \mathrm{e}^{\mathrm{i}\pi(h+k)}\right|^2 = \left|\tfrac{1}{2}f_{\mathrm{Cu}} - f_{\mathrm{K}}\theta\right|^2, \tag{3}$$

indicating a decrease in the intensity with increasing coverage θ. Time dependences of the coverage can be fitted to the data. In Fig. 1 the solid line shows a fit where the coverage is given by:

$$\theta(t) = \theta_{\max}(1 - \mathrm{e}^{-(t-t_0)/\tau}), \tag{4}$$

where $\theta_{\max}$ is the maximum K coverage (about 0.30 ML) and t_0 is the time at which the intensity begins to decrease. The parameter τ describes the time after which $1 - 1/\mathrm{e}$ of the $\theta_{\max}$ sites are occupied. In the present case the optimum choice was $\tau \approx 16.8$ s.

Assuming that only hollow sites are occupied the simulation fits the experimental data quite well up to the minimum at $t = 46$ s after the evaporation was started. This corresponds to a coverage of about 0.25 ML. However, it should be noted that on the basis of the present data the detailed analysis of the adsorption kinetics is not unique. The curvature of the intensity curve near the intensity minimum might be also explained by the the (partial) occupation of other than hollow sites, leading to an adlayer scattering that has no counterphase contribution. This means that a constant sticking coefficient up to a maximum coverage is still possible.

Independent of this, the decrease in the intensity at $(100)_t$ to roughly 50% of the uncovered Cu(001) surface at a coverage of up to 0.25 ML (no ordered superstructure formed) can only be explained by almost total occupation of hollow sites. This is directly evident from Eq. (3) using the scattering factors for Cu and K ($f_{\mathrm{Cu}} = 23.7$ and $f_{\mathrm{K}} = 13.9$ at $(100)_t$ [31]). After stopping evaporation the K atoms remain in the hollow sites (lower curve in Fig. 3a). This has also been confirmed during the measurement of the truncation rods (see below), which takes several hours.

Above about 0.25 ML the formation of the quasi-hexagonal superstructure sets in, showing up in the increase in the $(10, 0.05)_t$ intensity. We made no attempt to fit the time dependence of the intensity since there are too many free parameters that have to be taken into account. Instead, we calculated the intensity assuming the commensurate c(2 × 10) structure labeled C1 by Aruga et al. [22]. This is shown by the dotted line in Fig. 3(a). The registry of the C1 structure relative to the Cu(001) substrate is characterized by the occupation of substrate hollow sites by the adatoms at (0, 0) and (1/2, 1/2) within the c(2 × 10) unit cell, as shown in Fig. 2. The remaining disagreement observable in Fig. 3(a) can be explained by a modulation of the structure; this means that the structure formed is not exactly a commensurate c(2 × 10) structure, but is incommensurate. According to Toney et al. [32] this influences the truncation rod intensity as well. This will be discussed in more detail in Section 5.

In a second experiment Cs was evaporated on Cu(001). There is a remarkable difference as compared to the adsorption of K as can be seen in Fig. 3(b). After starting the evaporation the $(10\,0.05)_t$ truncation rod intensity decreases to about 60% of the initial value and remains constant. The intensity decrease to 60% is attributed to the formation of a superstructure very close to the commensurate C1 structure (Fig. 2). The solid line in Fig. 3(b) represents a simulation assuming the formation of the C1 structure. In addition, the filled symbols indicate the intensity (right

scale) of the first-order superlattice reflection $(0.0\,0.607\,0.05)_t$. The ideal C1 structure corresponds to a peak position at $k = 0.600$ reciprocal lattice units (rlu)

In order to fit the time dependence of the truncation rod intensity we have used the power law ansatz:

$$\theta(t) = \theta_{max}\left(\frac{t - t_0}{\Delta t}\right)^{\beta}. \quad (5)$$

Again we have assumed $\theta_{max} = 0.30$ ML, the theoretical coverage of the C1 structure. The parameter Δt represents the time for complete coverage of the surface (i.e. to evaporate 0.30 ML Cs) and t_0 marks the start of the intensity reduction. The exponent β describes the curvature of the curve. We have assumed that the coverage θ describes the fraction of the surface that is covered by the superstructure. From the fit we obtain $\beta \approx 2$.

There is no simple way to interpret this behavior. The shape of the intensity function seems to indicate an increasing sticking coefficient with coverage. This appears to be implausible and we may assume that the t^2 increase in the C1 contribution with time might be explained by a coverage-dependent ordering of small islands which finally coalesce.

An unambigous description of the adsorption behavior cannot be extracted in detail on the basis of the present X-ray data. Nevertheless, we can state that in contrast to the adsorption mechanism of K the unique occupation of hollow sites up to a coverage of about 0.20–0.25 ML has not been observed with Cs. Due to its larger scattering factor ($f_{Cs} = 44.1$) the decrease in the $(10\,0.05)_t$ truncation rod intensity for hollow-site adsorption is expected to be significantly larger than for K, as shown in Fig. 3(b). Therefore, one might speculate that the main difference between the adsorption behavior of K and Cs is that up to about 0.20–0.25 ML K atoms adsorb in hollow sites while Cs atoms form small, locally ordered clusters of the quasi-hexagonal C1 structure which grow and coalesce with increasing coverage. This difference can be rationalized in terms of the different sizes and polarizability of K (4s valence electron, $r_{ion} = 1.33$ Å, $r_{cov} = 2.38$ Å) and Cs (6s valence electron, $r_{ion} = 1.67$ Å, $r_{cov} = 2.68$ Å), both of which make the Cs atoms less sensitive to the substrate corrugation potential. The analysis of the superlattice reflections in Section 5 will give a consistent picture of this structure model.

4. Analysis of the truncation rods

Structure information normal to the sample surface can only be obtained by the analysis along $q_\perp$, the reciprocal lattice rod normal to the sample surface. In Fig. 4 we show on a logarithmic scale the $(10l)_t$ truncation rod intensity measured for uncovered (open symbols) and Cs-covered (filled symbols) Cu(001) surfaces after the formation of the quasi-hexagonal superstructure. In order to clarify the intensity modulation along $q_\perp$, we have plotted in Fig. 5 the ratio I_{cov}/I_{clean} for the Cs sample. The error bars are determined on the basis of the counting statistics and by averaging over symmetry-equivalent rods.

As discussed in Section 3, there is an intensity reduction to about 60% of the uncovered sample for $q_\perp \approx 0$. Close to the Cu substrate bulk Bragg point at $q_\perp/c^* = 1$ ($c^* = 0.276$ Å^{-1}) the ratio converges to 1, since this corresponds to the condition where the substrate layers scatter in phase, thus making the Cs monolayer contribu-

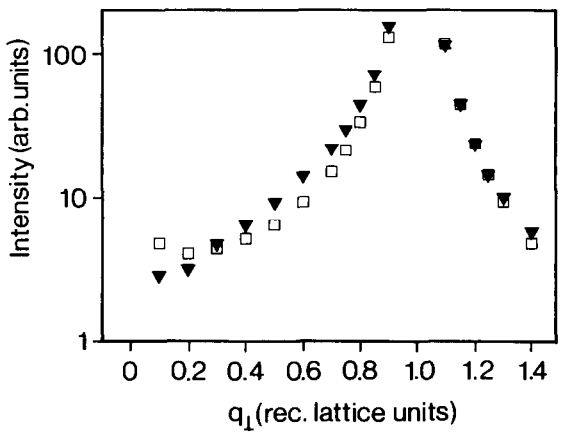

Fig. 4. Intensity of the clean (open symbols) and Cs-covered (filled symbols) Cu(001) surfaces measured as a function of $q_\perp$ along the $(10l)_t$ truncation rod. The corresponding ratio is shown in Fig. 5.

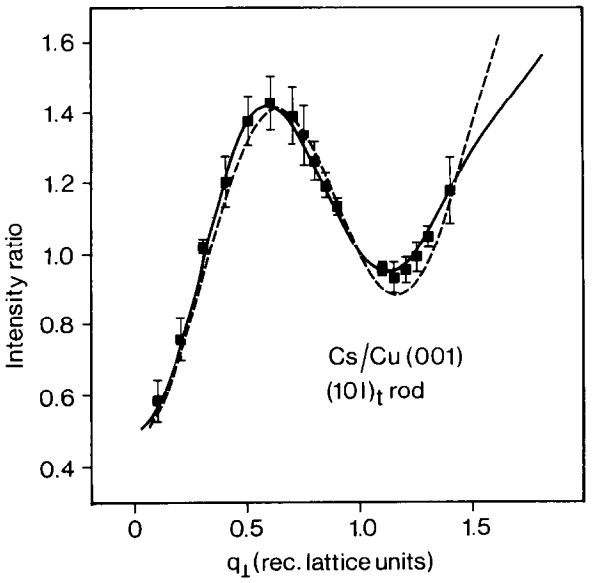

Fig. 5. Ratio I_{cov}/I_{clean} between Cs-saturated (≈ 0.30 ML) and clean Cu(001) surfaces along the $(10l)_t$ truncation rod. From the modulation frequency an average adsorption height $d_\perp = 2.94(15)$ Å is determined. The best fit (solid line) also takes account of substrate interlayer relaxations upon alkali adsorption. Neglecting the relaxations leads to the dashed line (see text).

tion negligible. We fitted the measured intensity modulation assuming the C1 structure with the atoms at (0, 0) and (1/2, 1/2) located in the hollow sites of the Cu substrate as shown in Fig. 2. A change in the Cu interlayer distances upon Cs adsorption was also allowed. Following Davis and Noonan [33], we used the interlayer spacings $d_{12} = 1.778$ Å and $d_{23} = 1.839$ Å for clean Cu(001).

The optimum two-parameter model (unweighted residuum $R_u = 0.016$ [34]) was obtained for Cs atoms at $d_\perp = 2.94(15)$ Å above the surface and relaxing the substrate interlayer spacings to the bulk value of $d_{Cu} = 1.808$ Å. Note that the adsorption height is an average value only, since both hollow sites and asymmetric sites are occupied (see Fig. 2). In the present investigation the resolution along $q_\perp$ is not sufficient to distinguish between these sites on the basis of their different $d_\perp$ values.

Within the hard-sphere model, the derived average adsorption height corresponds to values for the Cs radius between $r_{Cs} = 2.18(13)$ Å for adsorption in hollow sites and $r_{Cs} = 1.93(14)$ Å for occupation of bridge sites. The bridge site is the uppermost possible site for the Cs atoms.

The effect of the substrate interlayer relaxation is important as well. The dashed line in Fig. 5 corresponds to the fit where the interlayer spacings of the uncovered curve has been kept constant. At intermediate and high $q_\perp$, remarkable deviations from the experimental data are observed, showing up in a considerably worse fit ($R_u = 0.038$).

Our results are in good agreement with those of various other investigations on Cs adsorption on metals [6–8] leading to an effective Cs radius in the range 1.73(5) Å to 1.90(8) Å for top site adsorption and 2.10(6) Å to 2.17(2) Å for hollow-site adsorption. These values are about halfway between the ionic (1.67 Å) and the covalent (2.67 Å) radius of Cs. This fits into the picture of partial electron transfer to the substrate.

Coverage-dependent measurements were made for K adsorption. In the lower panel of Fig. 6 we show the ratio of the $(10l)_t$ truncation rod intensity obtained after stopping evaporation at the minimum of the $(10\,0.05)_t$ intensity (see Fig. 3a) corresponding to a coverage of about 0.25 ML. The solid line through the data points is a fit assuming K atoms are located in hollow sites at an adsorption height of $d_\perp = 2.25(15)$ Å, corresponding to an effective radius of $r_K = 1.6(1)$ Å, which is close to the ionic K radius (1.33 Å).

As for Cs adsorption, the substrate interlayer spacings are assumed to relax to the bulk value in order to fit the data adequately at $q_\perp/c^* > 1$. Again, neglecting this effect leads to a considerably worse fit, as can be seen from the dashed curve ($R_u = 0.064$, compared with $R_u = 0.034$ for the solid curve). The upper panel of Fig. 6 shows the ratio of the $(10l)_t$ truncation rod intensity obtained after continued evaporation leading to the formation of the quasi-hexagonal superstructure. As shown in Fig. 3(a), in this case the intensity increases to about 75% of the uncovered Cu surface.

The solid line represents the calculation assuming the commensurate C1 structure using an (average) adsorption height $d_\perp = 2.10(10)$ Å.

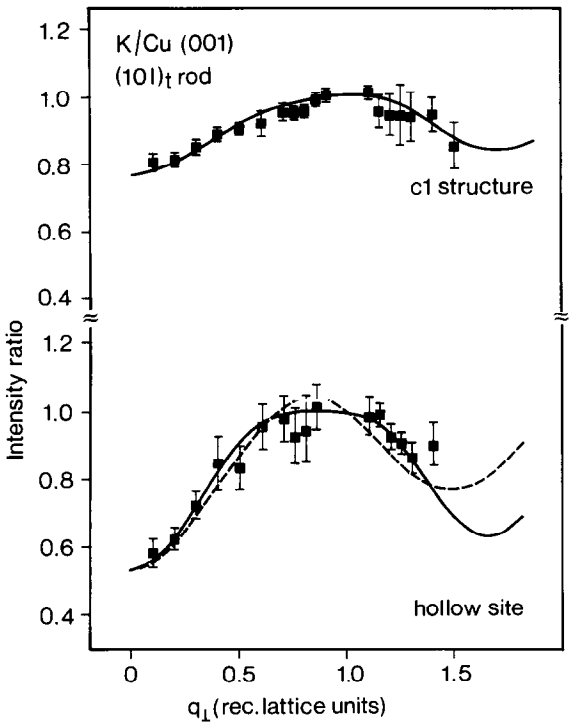

Fig. 6. Ratio I_{cov}/I_{clean} between the K-covered and the clean Cu(001) surfaces along the $(10l)_t$ truncation rod. Lower panel, data obtained after stopping evaporation at the minimum of the uptake curve (lower curve in Fig. 3a); upper panel, intensity ratio measured after formation of the incommensurate superstructure corresponding to the saturation of the $(100.05)_t$ truncation rod intensity (upper curve in Fig. 3a). In both cases the optimum fits (solid lines) lead to about $d_\perp = 2.10$–2.25 Å. The dashed line is a fit neglecting substrate interlayer relaxations (see text).

Within the error bars this is equal to the adsorption height derived for the K atoms located in the hollow sites. It is important to note that the superstructure is found to be modulated, which also affects the intensity of the truncation rods. However, the average adsorption height is only determined by the frequency of the intensity modulation along $q_\perp$. As a result of these investigations we can state that we cannot observe any coverage-dependent change in the adsorption height for K adsorption on Cu(001) within the error limits of about ± 0.15 Å. This result has to be compared with those of our previous investigation [20]. At a coverage of about 0.14 ML K adsorbed on Cu(001) we found $d_\perp = 2.1(4)$ Å associated with an effective radius $r_K = 1.5(3)$ Å. Although the error bars of these data were considerably larger than those shown here, they are in quite good agreement. Also, our results for the K adsorption lead to a considerably lower effective radius of $r_K = 1.6(1)$ Å than those derived from various LEED investigations: 1.96(5) Å [13] and 1.87(5) Å [10] for the K/Ni(001) c(4 × 2) and the K/Co(10$\bar{1}$0) c(2 × 2) structures, respectively, in which hollow sites are occupied by the adsorbate. On the other hand, in one investigation based on measurements of specular LEED intensities, Fisher et al. [35] derived $r_K = 1.46(10)$ Å for K/Ni(111), independent of coverage.

5. Analysis of the superlattice reflections

The analysis of the fractional-order superlattice reflections provides additional information about the structure of the ordered adlayers. In Fig. 7 a schematic view of the reciprocal lattice corresponding to the commensurate C1 structure is shown. Large circles represent the integer-order

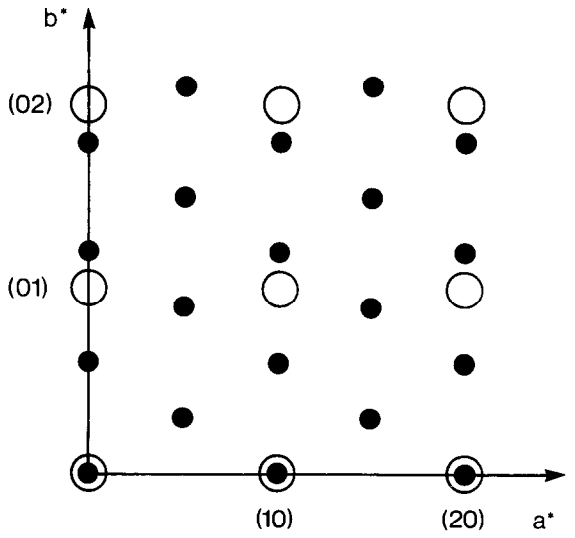

Fig. 7. Schematic representation of the reciprocal lattices for K/Cu(001) and Cs/Cu(001) assuming the commensurate C1 structure shown in Fig. 2. Large open circles represent integer-order Cu substrate reflections; small filled circles indicate superlattice reflections due to the alkali adlayer. Only one of the two possible domains is shown.

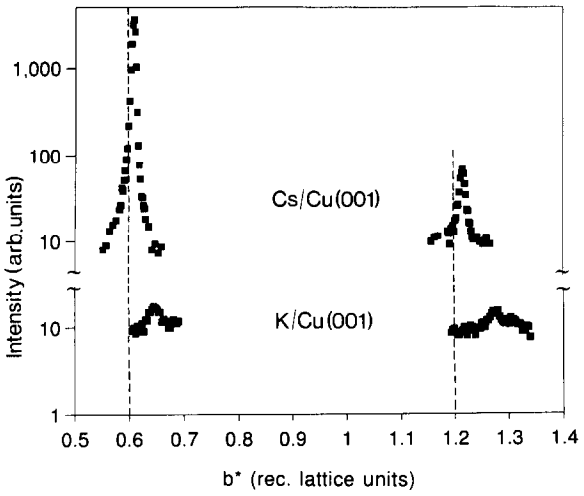

Fig. 8. First- and second-order superlattice reflections for Cs/Cu(001) (upper level) and K/Cu(001) (lower level) along the b^* reciprocal axis (see Fig. 7) shown on a logarithmic scale. Note especially that the second- to first-order intensity ratio for K/Cu(001) is longer than that for the Cs/Cu(001) system.

truncation rods, small circles indicate superlattice reflections related to one of the two equally probable domains.

In Fig. 8 the measured intensities of the first- and second-order reflections along the b^* reciprocal axis are plotted on a logarithmic scale for both the Cs/Cu(001) and K/Cu(001) samples. Both adsorbate systems were found to be commensurate along the a-axis but incommensurate along the b-axis (see Fig. 2). However, there are several important differences between the Cs/Cu(001) and the K/Cu(001) adsorption system.

After evaporation of Cs at about 303 K the first-order superlattice reflection was found at $k = 0.607$ rlu (reciprocal lattice unit), which is close to the commensurate position at 0.600 rlu corresponding to the C1 structure shown in Fig. 2. By keeping the evaporation rate at a constant (low) level and varying the substrate temperature, it was possible to continuously shift the reflections between $k = 0.586$ and 0.625 rlu, as depicted in Fig. 9. The numbers indicate the sequence of the measurements. The shift of the superlattice reflections was also possible by changing the evaporation rate, although the effect was less pronounced.

We could not find significant changes in the reflection profiles as a function of the peak position. In addition, there is no "lock-in" at the commensurate position $k = 0.600$ rlu. In summary, this indicates a continuous expansion and contraction of the adlayer unit mesh rather than a commensurate–incommensurate transition. Importantly, the formation of the commensurate C2 phase (2×3 superstructure) reported by Aruga et al. [22] for K/Cu(001) corresponding to a first-order reflection at $k = 0.666$ rlu was not observed. Instead, the Cs adlayer forms a rotated phase above $k = 0.625$ rlu. Further details of this result will be discussed elsewhere [36].

In contrast to the Cs/Cu(001) system, after adsorption of K on Cu(001) the first-order reflection was found at $k = 0.646$ rlu. Neither the peak position nor its intensity could be varied appreciably by changing the preparation conditions (substrate temperature 330 K) within the small limits that led to an ordered superstructure at all. As for the Cs/Cu(001) system a continuous supply of alkali atoms was necessary to stabilize the superstructure.

More details about the modulation of the incommensurate superstructures can be derived from the analysis of the reflection intensities. In the following we use a generalized version of the formalism used by Toney et al. [32].

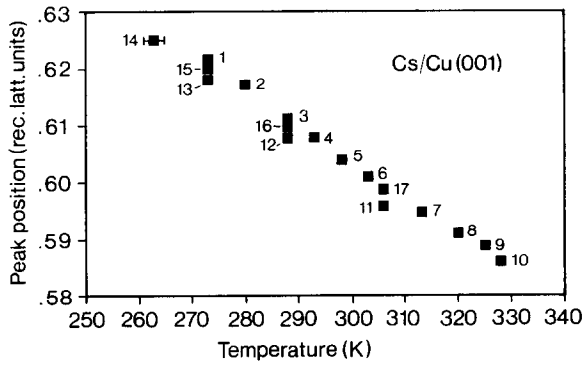

Fig. 9. First-order peak position as a function of substrate temperature for Cs/Cu(001). The numbers indicate the sequence of measurement. The peak position corresponding to the commensurate C1 structure is 0.600.

The substrate-induced spatial modulation of the jth adatom, $\boldsymbol{u}_j$, can be expanded in terms of the in-plane substrate wavevectors $\boldsymbol{G}$:

$$\boldsymbol{u}_j = \sum_{-\infty}^{\infty} \boldsymbol{u}_G \, e^{i\boldsymbol{G}\boldsymbol{R}_j}. \tag{6}$$

The vector $\boldsymbol{R}_j$ denotes the (average) position of the jth adatom in the absence of the substrate. For the total scattered amplitude of the modulated adlayer, $A(\boldsymbol{Q})$ we can write:

$$A(\boldsymbol{Q}) = f(\boldsymbol{Q}) \sum_j e^{-i\boldsymbol{Q}\cdot(\boldsymbol{R}_j + \boldsymbol{u}_j)}. \tag{7}$$

For convenience, we choose the modulation to be centrosymmetric with $\boldsymbol{u}_j = -\boldsymbol{u}_{-j}$ so that $\boldsymbol{u}_G$ becomes purely imaginary. Inserting Eq. (6) into Eq. (7) and using the Anger–Jacobi expansion of the integer-order Bessel functions $J_p(X)$:

$$e^{i\boldsymbol{Q}\cdot\boldsymbol{u}_G \sin \boldsymbol{G}\boldsymbol{R}_j} = \sum_p J_p(\boldsymbol{Q}\cdot\boldsymbol{u}_G) \, e^{ip\boldsymbol{G}\cdot\boldsymbol{R}_j}, \tag{8}$$

we obtain for the total amplitude $A(\boldsymbol{Q})$:

$$A(\boldsymbol{Q}) = f(\boldsymbol{Q}) \sum_j \sum_G \sum_p J_p(\boldsymbol{Q}\cdot\boldsymbol{u}_G) \, e^{-i\boldsymbol{R}_j\cdot(\boldsymbol{Q}-p\boldsymbol{G})}. \tag{9}$$

Setting $p = 0$ and truncating the series over G at $G = 1$, i.e. $\boldsymbol{G} = (0, 1)$ we obtain the amplitudes of the superlattice reflections as a function of the first-order Fourier component of the substrate-induced modulation $\boldsymbol{u}_{01}$:

$$A_0(\boldsymbol{Q}) = f(\boldsymbol{Q}) J_0(\boldsymbol{Q}\cdot\boldsymbol{u}_{01}), \tag{10}$$

where $J_0(x)$ is the zero-order Bessel function. Due to the modulation of the adlayer the superlattice reflections corresponding to the average structure lose intensity, which is transferred to the satellite reflections. Since the modulation wavevectors are commensurate with the substrate periodicity the satellites interfere with the integer-order truncation rods. For example, the amplitude at (010) along the (01l) truncation rod is given by:

$$A_{CTR}(\boldsymbol{Q}) = F_{CTR} - \theta f(\boldsymbol{Q}) J_1(\boldsymbol{G}\cdot\boldsymbol{u}_{01}), \tag{11}$$

where $J_1(x)$ is the first-order Bessel function and θ is the coverage. The sign determines the phase of the adlayer relative to the substrate. It should also be noted that although we measured the (10) truncation rod we nevertheless obtain information about the $\boldsymbol{u}_{01}$ modulation amplitude, since there are two equi-probable domains of the alkali adlayer on the surface.

Table 2
Structure factor intensities for the first- and second-order superlattice reflections as derived for K/Cu(001) and Cs/Cu(001)

	Cs/Cu(001)	K/Cu(001)
$\lvert F_1 \rvert^2$	451 (5)	4.2 (0.7)
$\lvert F_2 \rvert^2$	56 (7)	7.5 (2.0)

Table 2 lists the derived structure factor intensities after correction for instrumental parameters. The most interesting observation is that for K/Cu(001) the second-order reflection intensity is more intense than the first-order intensity, although the structure is primitive and to first order the intensities are expected to fall off with the squared scattering factor $|f(Q)|^2$. This can only be explained by a large modulation amplitude u_{01} for the K adsorbate layer. In Fig. 10 the squares represent as a function of the modulation amplitude u_{01} the calculated intensity ratios between the first- and the second-order superlattice

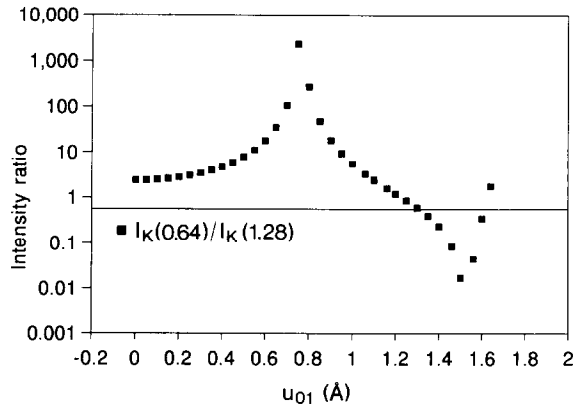

Fig. 10. Calculated ratio between first- and second-order superlattice reflections for K/Cu(001) as a function of u_{01}. The experimental ratio is indicated by the solid horizontal line. The fit of the data is possible for $u_{01} \approx 1.30$ Å. The second solution $u_{01} \approx 1.65$ Å can be excluded from the analysis of the truncation rod data.

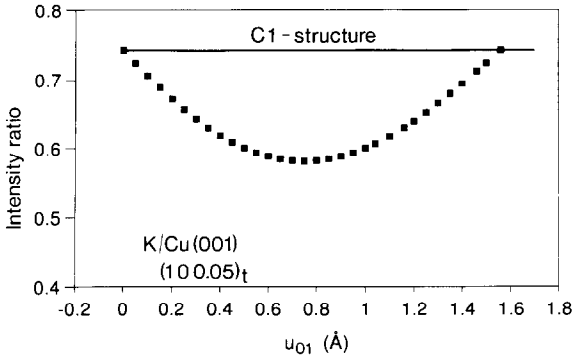

Fig. 11. Calculated $(100.05)_t$ truncation rod intensity ratio between K-covered and clean Cu(001) samples as a function of u_{01}. The calculated intensity ratio assuming the unmodulated commensurate C1 structure is shown by the solid horizontal line.

reflection of the K adlayer. The horizontal line represents the measured ratio, $I_K(k = 0.64)/I_K(k = 1.28) = 0.56(18)$, which can be fitted by a modulation amplitude $u_{01} = 1.29(3)$ Å. This is consistent with the modulation of the $(100.05)_t$ truncation rod intensity for K/Cu(001) shown in Fig. 3(a). The dotted line shows the calculated intensity assuming the unmodulated C1 structure (coverage $\theta = 0.30$ ML and $u_{01} = 0$). Note, that the intensity calculated for the C1 structure is exactly halfway between the intensity calculated for the clean sample and for the adsorbate structure where all K atoms ($\theta = 0.30$ ML) are assumed to reside in hollow sites. This is due to the fact that for the C1 structure only one of the two domains contribute to the scattering, whereas both domains contribute in the case of unique hollow-site adsorption.

As shown in Fig. 3(a) the experimental intensity is about 10–15% less than that calculated for the ideal C1 structure. This observation can also be explained by the modulation of the K-adlayer. In Fig. 11 we show the calculated intensity ratio between K-covered and clean Cu(001) as a function of u_{01}. In the case of $u_{01} = 0$ the intensity ratio is about 0.75, as in Fig. 3(a), but increasing u_{01} leads to an oscillating intensity behavior according to Eq. (11). For $u_{01} \approx 1.3$ Å we obtain an intensity reduction of about 14% relative to the unmodulated structure. This is in agreement with our observation. Since the truncation rod intensity is reduced ($u_{01} > 0$) we conclude that the K atoms tend to move into the hollow sites along the *b*-direction (see Fig. 2).

From inspection of Fig. 10 it can be seen that the experimental ratio $I_K(0.64)/I_K(1.28) = 0–56$ has a second solution for $u_{01} \approx 1.65$ Å. However, this result would be inconsistent with the $(10, 0.05)_t$ truncation rod intensity.

For Cs/Cu(001) the same analysis can be performed leading to a modulation amplitude u_{01} of at most 0.2 Å indicating only minor modulation of the adlayer. The experimental ratios between the superlattice reflection intensities of Cs and K, $I_{Cs}(0.61)/I_K(0.64) = 107(17)$ and $I_{Cs}(1.22)/I_K(1.28) = 7.5(2.2)$ are also consistent with this picture. For the Cs/Cu(001) system thermal disorder is dominant.

From the temperature-dependent analysis of 12 and 14 symmetry-independent superlattice reflections we found strong anisotropic temperature factors characterized by mean squared vibration amplitudes of $\langle u_{11}^2 \rangle = 0.10(2)$ Å^2 and $\langle u_{22}^2 \rangle = 0.16(2)$ Å^2 at 190 K and of $\langle u_{11}^2 \rangle = 0.18(2)$ Å^2 and $\langle u_{22}^2 \rangle = 0.29(2)$ Å^2 at 303 K. The subscripts 11 and 22 indicate the commensurate and incommensurate directions, respectively. Debye temperatures of about $\Theta_{11} = 44$ K and $\Theta_{22} = 34$ K have been calculated from the vibration amplitudes.

6. Summary and conclusions

Using the intensity modulation along the crystal truncation rods we have investigated the adsorption and the structure of Cs and K adlayers on Cu(001). Due to the different sizes and polarizability of the adatoms we observe remarkable differences. While K adsorbs in fourfold hollow sites up to about 0.25 ML, Cs atoms are found to occupy different adsorption sites, even at low coverage. One possible interpretation is the formation of locally ordered islands of the quasi-hexagonal superstructure, which grow with increasing coverage.

The analysis of the crystal truncation rods provides information about the adsorption height of

the adatoms. For Cs we derive $d_{\perp} = 2.94(15)$ Å, corresponding to an effective radius in the range 1.93–2.18 Å, which is in between the ionic (1.67 Å) and the covalent (2.67 Å) radius. For K we find, independent of the coverage, an adsorption height of about 2.10 Å leading to $r_K = 1.6$ Å, which is close to the ionic radius (1.33 Å).

The conventional picture of charge transfer and charge back-donation at high coverage would require an ionic adsorbate at low and intermediate coverages and a more metallic alkali layer close to the completion of the substrate surface. The constant adsorption height of the K adatoms with increasing coverage seems to contradict this picture. A more sophisticated view of the alkali adsorption is needed to explain the workfunction changes.

Further, the "hard-sphere" model used to derive the effective radii appears too simple for these complicated electronic structures. Several theoretical attempts to analyze the alkali metal/metal chemisorption systems have recently been made. Using Hartree–Fock SCF cluster calculations, Pacchioni et al. [5] showed that K chemisorbed on the Cu(001) is highly ionic. The ionicity of the adatom leads to a polarization of the Cu charge density leading to a considerable charge accumulation between the surface and the positive ion that should not be interpreted as the formation of a covalent bond. However, the equilibrium distance derived by the authors is close to 3 Å, significantly larger than all results based on experimental investigations.

We have also investigated the ordered superstructures that form at saturation coverage. On the basis of the results the systems Cs/Cu(001) and K/Cu(001) can be viewed as limiting cases for strong adsorbate–adsorbate interaction relative to the adsorbate–substrate interaction and vice versa. The quasi-hexagonal Cs superlattice could be continuously expanded and contracted depending on the adlayer density. The static modulation of the Cs adlayer was found to be small; the first-order Fourier component of the substrate-induced modulation, u_{01}, is at most 0.2 Å.

In contrast, the K-adlayer is strongly modulated. Both Shrimpton et al. [37] and Fisher and Diehl [38] have investigated uniaxially incommensurate phases of alkali atoms on fcc (001) faces by molecular dynamics calculations. They discuss in detail the domain wall characteristics depending on the relative strength between the adsorbate–adsorbate dipole interaction and the adsorbate–substrate interaction due to the substrate corrugation potential. The system K/Cu(001) is representative for the case of weak adsorbate–adsorbate dipole interaction and strong influence of the substrate corrugation potential corresponding to $C \leq 10$ in Ref. [37]. Shrimpton et al. also discuss for the (2×3) phase [39] (which corresponds to the C2 phase in Aruga's nomenclature [22]) a configuration consisting of a mix of $c(4 \times 2)$ and $c(2 \times 2)$ structures.

Using this structure model and recalling that the (average) structure determined for K/Cu(001) is close to the C2 structure (first-order reflection at $k = 0.646$ as compared to $k = 0.666$ for the C2 structure) the derived first-order modulation amplitude $u_{01} \approx 1.30$ Å appears to be reasonable since the shift of the K atoms from their average position to the hollow sites in order to form the $c(4 \times 2)$ and the $c(2 \times 2)$ structures are of the same order of magnitude. Such large modulations should also be evident in the reflection profiles, but in the present experiments the reflection intensities were too low to obtain suitable counting statistics

7. Acknowledgement

We (H.L.M. and J.W.) would like to thank AT&T for providing access to the beamline X16 A and their hospitality during our visit in Brookhaven. The support of this work by the Bundesministerium für Forschung und Technologie under grant No. 05464IAB8 is gratefully acknowledged. Work at the NSLS is supported by the US Department of Energy under DE-AC 012-76CH0016. Partial support also came from the University of Illinois Materials Research Laboratory under DEFG02-91ER45439. The authors thank R. Wunderlich for carefully preparing the drawings.

8. References

[1] I. Langmuir and K.H. Kingdon, Phys. Rev. 21 (1923) 380.

[2] H. Ishida, Phys. Rev. B 38 (1988) 8006;
H. Ishida, Phys. Rev. B 42 (1990) 10899.

[3] D.M. Riffe, G.K. Wertheim and P.H. Citrin, Phys. Rev. Lett. 64 (1990) 571.

[4] M. Scheffler, Ch. Droste, A. Fleszar, F. Máca, G. Wachuta and G. Barzel, Physica B 172 (1991) 143.

[5] G. Pacchioni and P.S. Bagus, Surf. Sci. 269/270 (1992) 669; Surf. Sci. 286 (1993) 317.

[6] C. von Eggeling, G. Schmidt, G. Besold, L. Hammer, K. Heinz and K. Müller, Surf. Sci. 221 (1989) 11.

[7] H. Over, H. Bludau, M. Skottke-Klein, G. Ertl, W. Moritz and C.T. Campbell, Phys. Rev. B 45 (1992) 8638.

[8] S.Å. Lindgren, L. Wallden, J. Rundgren, P. Westrin and J. Neve, Phys. Rev. B 28 (1983) 6707.

[9] C.J. Barnes, P. Hu, M. Lindroos and D.A. King, Surf. Sci. 251/252 (1991) 561.

[10] B.A. Hutchins, T.N. Rhodin and J.E. Demuth, Surf. Sci. 54 (1976) 419.

[11] G. Besold, Th. Schaffroth, K. Heinz, G. Schmidt and K. Müller, Surf. Sci. 189/190 (1987) 252.

[12] D. Fisher, S. Chandavarkar, I.R. Collins, R. Diehl, P. Kaukasoina and M. Lindroos, Phys. Rev. Lett. 68 (1992) 2786.

[13] U. Muschiol, P. Bayer, K. Heinz, W. Oed and J.B. Pendry, Surf. Sci. 275 (1992) 185.

[14] D. Adler, I.R. Collins, K. Ding, S. Chandavarkar, X. Liang, S. Murray, G.S. Leatherman, P.D. Johnson, R. McGrath, R.D. Diehl and P.H. Citrin, unpublished.

[15] M. Gierer, H. Bludau, T. Hertel, H. Over, W. Moritz and G. Ertl, Surf. Sci. Lett. 279 (1992) L170.

[16] C. Stampfl, M. Scheffler, H. Over, J. Burchardt, M. Nielsen, D.L. Adams and W. Moritz, Phys. Rev. Lett. 67 (1992) 1532.

[17] H. Wedler, M.A. Mendez, P. Bayer, U. Löffler, K. Heinz, V. Fritsche and J.B. Pendry, Surf. Sci. 293 (1993) 47.

[18] R. Feidenhans'l, Surf. Sci. Rep. 10 (1989) 105.

[19] I.K. Robinson, in: Handbook of Synchrotron Radiation, Vol. 3, Eds. G.S. Brown and D.E. Moncton (Elsevier, Amsterdam, 1991) p. 221.

[20] H.L. Meyerheim, I.K. Robinson, V. Jahns, P.J. Eng and W. Moritz, Z. Kristallogr. 208 (1993) 73.

[21] G.M. Lamble, R.S. Brooks, D.A. King and D. Norman, Phys. Rev. Lett. 61 (1988) 1112.

[22] T. Aruga, H. Tochihara, and Y. Murata, Surf. Sci. 158 (1985) 490.

[23] C.A. Papageorgopoulos, Phys. Rev. B 25 (1982) 3740.

[24] J. Cousty, R. Riwan and P. Soukiassian, Surf. Sci. 152/153 (1985) 297.

[25] M. v Laue, Ann. Phys. 26 (1936) 55.

[26] I.K. Robinson, Phys. Rev. B 33 (1986) 3830.

[27] S.R. Andrews and R.A. Cowley, J. Phys. C (Solid State Phys.) 18 (1985) 6427.

[28] We use a sample setting corresponding to a primitive (1×1) surface unit cell leading to a tetragonal bulk unit cell. This setting is related to the face-centered surface unit cell (cubic bulk unit cell) by the transformations: $[100]_t = 0.5\cdot\{[100]_c + [010]_c\}$, $[010]_t = 0.5\cdot\{[100]_c - [010]_c\}$ and $[001]_t = [001]_c$.

[29] P.H. Fuoss and I.K. Robinson, Nucl. Instrum. Methods 222 (1984) 171.

[30] E. Vlieg, J.F. van der Veen, J.E. MacDonald and M. Miller, J. Appl. Crystallogr. 20 (1987) 330.

[31] D.T. Cromer and J.T. Waber, in: International Tables for X-Ray Crystallography, Eds. J.A. Ibers and W.C. Hamilton (Kynoch, Birmingham, UK, 1974) p. 71.

[32] M.F. Toney, J.G. Gordon, M.G. Samant, G.L. Borges, O.R. Melroy, L.-S. Kau, D.G. Wiesler, D. Yee and L.B. Sorensen, Phys. Rev. B 42 (1990) 5594.

[33] H.L. Davis and J.R. Noonan, Surf. Sci. 126 (1983) 245.

[34] In the present case the unweighted residuum, R_u, is defined by: $R_u = \Sigma \| Y_{obs} | - | Y_{calc} \| / \Sigma | Y_{obs} |$, where Y_{obs} and Y_{calc} correspond to observed and calculated ratios, respectively. The summation runs over all measured data points.

[35] D. Fisher, Zi-You Li and R. Diehl, Surf. Sci. 259 (1991) 85.

[36] P.J. Eng, I.K. Robinson, H.L. Meyerheim and J. Wever, to be published.

[37] N.D. Shrimpton, G.S. Welsh and J. Song, Phys. Rev. B 45 (1992) 1403.

[38] D. Fisher and R.D. Diehl, Phys. Rev. B 46 (1993) 2512.

[39] In Ref. [37] this structure is labeled by $c(2\times3)$, although this assignment is not strictly correct since the substrate symmetry has to be taken into account, leading only to a (2×3) superstructure.